Isospin Dependence of Incomplete Fusion Reactions at 25 MeV/Nucleon

F. Amorini,[1] G. Cardella,[2,*] G. Giuliani,[3] M. Papa,[2] C. Agodi,[1] R. Alba,[1] A. Anzalone,[1] I. Berceanu,[7] S. Cavallaro,[1,3] M. B. Chatterjee,[4] R. Coniglione,[1] E. De Filippo,[2] A. Di Pietro,[1] E. Geraci,[1,3] L. Grassi,[2,3] A. Grzeszczuk,[6] P. Figuera,[1] E. La Guidara,[2,8] G. Lanzalone,[1,9] N. Le Neindre,[5] I. Lombardo,[1,3] C. Maiolino,[1] A. Pagano,[2] S. Pirrone,[2] G. Politi,[2,3] A. Pop,[7] F. Porto,[1,3] F. Rizzo,[1,3] P. Russotto,[1,3] D. Santonocito,[1] P. Sapienza,[1] and G. Verde[2]

[1]*INFN Laboratori Nazionali del Sud, via Santa Sofia 44, Catania, Italy*
[2]*INFN, Sezione di Catania, Via Santa Sofia 64, Catania, Italy*
[3]*Department of Physics and Astronomy Catania University, Via Santa Sofia 64, Catania, Italy*
[4]*Saha Institute of Nuclear Physics, Kolkata, India*
[5]*LPC, CNRS/IN2P3, ENSICAEN, Université de Caen, F-14050 Caen cedex, France*
[6]*Institute of Physics, University of Silesia, Katowice, Poland*
[7]*National Institute for Physics and Nuclear Engineering "Horia Hulubei," Bucharest, Romania*
[8]*CSFNSM Via Santa Sofia 64, Catania, Italy*
[9]*"Kore" University, cittadella Universitaria, Enna, Italy*

(Received 8 September 2008; revised manuscript received 27 December 2008; published 19 March 2009)

^{40}Ca + ^{40,48}Ca, ^{46}Ti reactions at 25 MeV/nucleon have been studied using the 4π CHIMERA detector. An isospin effect on the competition between fusionlike and binarylike reaction mechanisms has been observed. The probability of producing a heavy residue is lower in the case of $N \approx Z$ colliding systems as compared to the case of reactions induced on the neutron rich ^{48}Ca target. Predictions based on constrained molecular dynamics II calculations show that the competition between fusionlike and binary reactions in the selected centrality bins can constrain the parametrization of the symmetry energy and its density dependence in the nuclear equation of state.

DOI: 10.1103/PhysRevLett.102.112701 PACS numbers: 25.70.Lm, 21.65.Ef, 21.65.Mn, 25.70.Jj

Collisions between heavy ions with different neutron-proton asymmetries offer a unique opportunity to study the equation of state of asymmetric nuclear matter [1–4]. Because of its impact on nuclear structure and on important properties of neutron stars, the density dependence of the symmetry energy has largely attracted the interest of the research community [2,5,6]. In this respect the isotopic composition of fragments produced in multifragmentation phenomena at intermediate beam energies (E/A = 20–100 MeV) provides important information on the symmetry energy [7]. One aspect not yet fully investigated is represented by the effect of the isospin asymmetry on the fate of hot nuclear systems. The combined effects of the symmetry energy and of the repulsive Coulomb interaction can significantly affect the rate of production of hot compound nuclei in heavy-ion reactions [8,9]. Once these hot nuclei are produced, their neutron-proton (N-Z) asymmetry is expected to play an important role in opening different decay channels affecting their limiting temperature [10–12]. Recent temperature measurements in the decay of projectile spectators at relativistic energies did not confirm the expected isotopic effects on limiting temperatures [13]. At lower beam energies, a small difference in the limiting giant dipole resonance excitation energy has been observed comparing a symmetric $N \sim Z$ system to a neutron rich system [14,15]. These findings stimulate further attempts to search for N-Z effects on nuclear dynamics and their important links to the density dependence of the nuclear symmetry energy.

In this work we explore isospin effects in the competition between two classes of reaction mechanisms. The first class produces one massive heavy residue (HR) and relatively small fragments in the final stage; the second class produces at least two heavy fragments with similar masses and lighter fragments. At the beam energy explored in the present work, incomplete fusion or massive transfer [16] mostly contribute to the first class of reaction mechanisms. In the second class one can have contributions from all kinds of binary collisions together with fusion-fission reactions. The results observed on the competition between these classes of reaction mechanisms are compared to simulations performed with a microscopic model with the aim of constraining the density dependence of the symmetry energy.

The experiment was performed at the INFN Laboratori Nazionali del Sud (LNS) with ^{40}Ca beams at 25 MeV/nucleon delivered by the LNS Superconducting Cyclotron. Reactions on self-supporting, metallic form, ^{48,40}Ca and ^{46}Ti isotopically enriched targets have been studied. The thicknesses of the targets were, respectively, 2.87, 1.24, and 1.06 mg/cm^2. Produced fragments were detected by the CHIMERA [17] 4π multidetector, consisting of 1192 silicon-CsI(Tl) telescopes, arranged in 26 rings covering 95% of 4π from 1° to 176°. The most forward

rings, up to 4.5°, were covered. The event trigger conditions of the experiment required at least three silicon detectors fired by fragments, with charge $Z > 1$, in order to remove the most peripheral collisions. The charge and mass of detected particles were determined by means of standard ΔE-E and fast-slow identification techniques [18]. Particle velocities were determined by time-of-flight (TOF) measurements performed using the cyclotron radio frequency as a reference time and the silicon detectors as stop signals [19]. The resulting TOF resolution is of the order of 1 ns, mostly due to beam time characteristics. Combining the TOF and energy measurements, the mass of particles stopped in silicon detectors was also evaluated. An overall mass resolution $\Delta M/M$ of the order of 5% [20] has been estimated for masses $A \sim 50$, i.e., the typical mass of HR fragments relevant to the analysis presented in this work. Because of handling difficulties, oxidation occurred in ^{40}Ca and ^{48}Ca targets. However, uninteresting reactions induced by the beam on oxygen contaminants in the targets have been isolated and removed from the data analysis by studying only complete events. These events were defined by requiring the sum of the charges of all detected fragments, $\sum Z_i$, to be larger than 80% of the total charge of the entrance channel, i.e., $\sum Z_i > 32$. Moreover, we required also the sum of all fragment momenta, $\sum P_i$, to be larger than 70% of the total momentum P of the projectile. Furthermore, events produced by a possible pileup of two or more reactions were excluded by requiring $\sum Z_i$ to be smaller than 40, for Ca targets, and smaller than 42, for Ti targets requiring also $\sum P_i$ to be not larger than P. Charged particle multiplicity distributions are shown in Fig. 1(e) for the ^{40}Ca + ^{48}Ca (full dots) and for ^{40}Ca + ^{46}Ti (shaded area histogram) reactions. The distribution obtained with N-Z symmetric ^{40}Ca targets, being very similar to that observed with ^{46}Ti targets, is not shown. The maximum in the multiplicity distributions is shifted back by one unit in the case of ^{48}Ca targets, probably due to a larger neutron emission probability. Taking into account this observation, in order to minimize contributions from very peripheral reactions, only events with a multiplicity of at least five charged particles, in the case of ^{48}Ca target, and six charged particles, in the case of ^{46}Ti and ^{40}Ca targets, have been selected. In order to isolate events where incomplete fusion occurs, we required the velocity of the second or third heaviest detected fragment to be larger than $0.13c$. In fact, in such kind of reactions, the portion of the projectile that does not fuse with the target is expected to move with a velocity close to that of the projectile. This selections strongly suppress events in which only a part of the target fuses while the remnant behaves like a spectator [16]; target spectators are in fact not detected and do not contribute to the $\sum Z_i$.

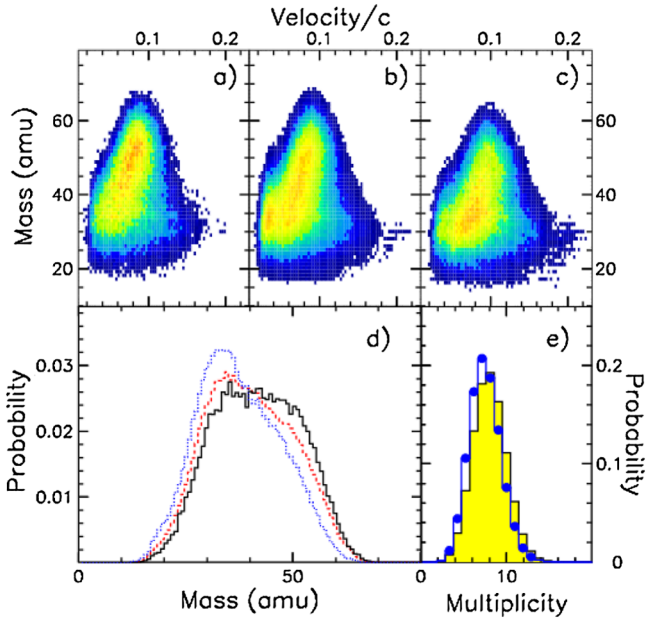

FIG. 1 (color online). Mass m_1 versus velocity v_1 of the largest fragment detected in the ^{40}Ca + ^{48}Ca (a), ^{40}Ca + ^{46}Ti (b), and ^{40}Ca + ^{40}Ca (c) reactions. (d) Projections on the mass axis for ^{48}Ca target (full line) ^{46}Ti target (dashed line), and ^{40}Ca target (dotted line). (e) Charged particle multiplicity in the reactions ^{40}Ca + ^{48}Ca (dotted histogram) and ^{40}Ca + ^{46}Ti (shaded area histogram).

Figures 1(a)–1(c) show the correlations between the mass m_1 and the velocity v_1 of the largest detected fragment in the reactions ^{40}Ca + ^{48}Ca, ^{40}Ca + ^{46}Ti and ^{40}Ca + ^{40}Ca, respectively. The distribution in Fig. 1(a) is peaked at velocities $v_1 \sim 0.09c$, close to the center of mass velocity of the ^{40}Ca + ^{48}Ca reaction ($V_{\text{c.m.}} = 0.105c$), and at masses $m_1 \sim 50$ amu. These large fragments are the HR remnants of incomplete fusion reactions. The distributions obtained for the other two reactions [Figs. 1(b) and 1(c)] regardless of their similarities, display some marked differences. Targetlike nuclei, with a velocity smaller than $0.04c$, are detected more copiously in the case of a ^{46}Ti target [Fig. 1(b)] than in the case of a ^{40}Ca target [Fig. 1(c)]. These heavy and slow targetlike fragments are mostly stopped in the thicker ^{48}Ca target and therefore they are not observed in Fig. 1(a). The fragment mass distributions of the three reactions are rather different. This can be better seen in Fig. 1(d) where the projections of the scatter plots (top panels) on their mass axis are shown (a cut at $0.04 < v_1/c < 0.15$ was used to exclude targetlike and projectilelike fragments). These distributions are peaked at smaller masses in the case of ^{46}Ti, ^{40}Ca targets (dashed line and dotted line, respectively) than in the case of a ^{48}Ca target (continuous line). A bump around mass $m_1 \sim 50$ is seen in reactions on a ^{48}Ca target, and gradually disappears when moving towards more symmetric ^{46}Ti to ^{40}Ca targets. In order to further explore mass correlations, and to give an operative definition of the two classes of reaction mechanisms that we want to investigate, we plot on the left-hand panels of Fig. 2, as dot histograms, the difference between the masses of the two largest fragments, $m_1 - m_2$, normalized to the mass m_{tot} of the entrance channels,

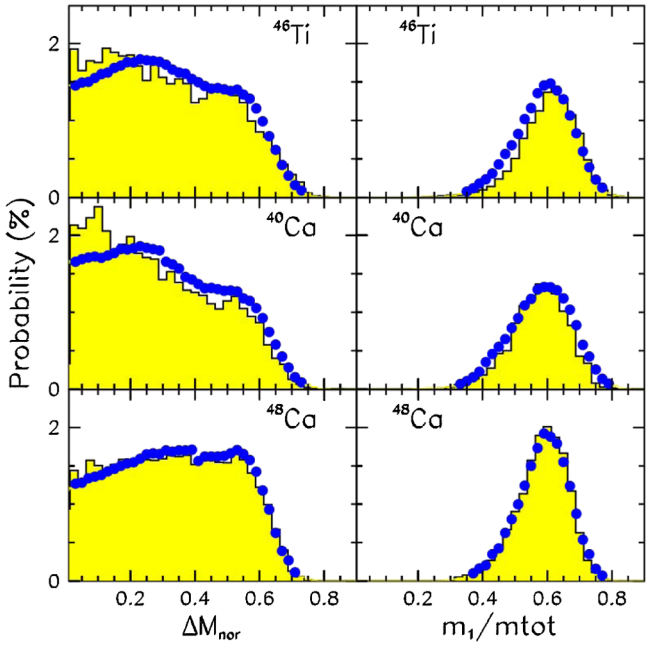

FIG. 2 (color online). Dot histograms: Probability plots of $m_1 - m_2$ and m_1 normalized to the total mass for the studied reactions. Shaded histogram: CoMD-II + GEMINI calculations. See text for details.

$\Delta M_{\mathrm{nor}} = (m_1 - m_2)/m_{\mathrm{tot}}$. In order to exclude targetlike contributions biased by differences in target thickness, only fragments having velocities greater than $0.04c$ have been taken into account. ΔM_{nor} minimizes the effects due to the mass difference between the three targets and enhances the effects due to their isotopic content. In these spectra one observes a local minimum around $\Delta M_{\mathrm{nor}} \approx 0.4$. We then use this value as an operative threshold between the two classes of investigated reaction mechanisms and assume that events with $\Delta M_{\mathrm{nor}} > 0.4$ ($m_2 < 16$ if $m_1 = 50$ with ^{48}Ca targets) belong to the first class mainly producing one HR. Comparing the three left-hand panels in Fig. 2 a clear enhancement at $\Delta M_{\mathrm{nor}} \sim 0.5$ in the case of reactions induced on ^{48}Ca targets is observed. On the other hand, in the case of $N \approx Z$ symmetric reactions ^{40}Ca + ^{40}Ca and ^{40}Ca + ^{46}Ti, the distribution is clearly pushed to low ΔM_{nor} values. A difference can be observed also in the mass distribution m_1/m_{tot} of the heavy residues shown in the right-hand panels of Fig. 2 for events selected with the condition $m_2 < 10$. A wider m_1/m_{tot} distribution is obtained with the $N \approx Z$ targets. This can be induced by the presence of larger fluctuations on the mass of the primary incomplete fused system or by a larger probability for this system to decay emitting complex fragments and thus displaying large variations in its final mass. The observed larger probability of producing heavy residues observed in ^{40}Ca + ^{48}Ca reactions and the smaller m_1 mass fluctuations may be connected to the larger neutron content of ^{48}Ca.

In fact, the neutron excess of the ^{40}Ca + ^{48}Ca system pushes the formed hot compound nucleus closer to the stability valley. On the contrary, the intermediate systems formed with the other two $N \approx Z$ targets are much closer to the proton drip line.

In order to go beyond this qualitative observation, and better investigate the mechanisms responsible for the observed effects and their links to the symmetry interaction, we compare experimental results to calculations performed with the CoMD-II (constrained molecular dynamics II) model [21]. In this model, the dependence of the isospin dependent interaction on the total overlap integral s between the wave packets is characterized by a form factor $F(s/s_{\mathrm{g.s.}})$ (the label g.s. corresponds to the ground state configuration) [22]. This form factor can be expressed, for compact configurations, as $F(s/s_{\mathrm{g.s.}}) = s/s_{\mathrm{g.s.}} F'(s/s_{\mathrm{g.s.}})$. Depending on the specific choice of $F'(s/s_{\mathrm{g.s.}})$, one can select a different stiffness of the density dependence of the symmetry energy. Specifically, we have used the following functional forms: $F'(s/s_{\mathrm{g.s.}}) = 2(s/s_{\mathrm{g.s.}})/(1 + s/s_{\mathrm{g.s.}})$ (Stiff1), $F'(s/s_{\mathrm{g.s.}}) = 1$ (Stiff2). $F'(s/s_{\mathrm{g.s.}}) = (s/s_{\mathrm{g.s.}})^{-1/2}$ (Soft) suggested from equation of state static calculations and widely used in Boltzmann-Uehling-Uhlenberg mean-field calculations [1,2]. The strength factor used for the symmetry interaction is 27 MeV [22]. In order to compare CoMD-II calculations with mean-field approaches that use as a fundamental quantity the one-body density ρ, we underline that the ratios $s/s_{\mathrm{g.s.}}$ and $\rho/\rho_{\mathrm{g.s.}}$ are equivalent within 1%. Another kind of functional for the form factor, which is widely used in the literature, is $\Phi(\gamma, s/s_{\mathrm{g.s.}}) = (s/s_{\mathrm{g.s.}})^{\gamma}$ where γ can be assumed as a measure of the degree of stiffness. We note that for the Stiff2 option the functional F and Φ are identical (with $\gamma = 1$). To compare with the functional Φ the other two options used in this Letter we can reasonably assume that the dynamical evolution of the system strongly depends on the value of the maximum density overlap, s_{max}, achieved during the first 100 fm/c. At this stage of the dynamical evolution of the system, at the investigated energy, the quantity $(s - s_{\mathrm{g.s.}})/s_{\mathrm{g.s.}}$ is relatively small ($\approx$10%–15%), so that one can approximate $F'(s/s_{\mathrm{g.s.}}) \approx 1 + \delta(s - s_{\mathrm{g.s.}})/s_{\mathrm{g.s.}}$. The form factors used in the case of Stiff1, Stiff2, and Soft isovector potentials correspond, respectively, to $\delta = 0.5$, $\delta = 0$, and $\delta = -0.5$. In the same limit it is easy to verify that $F'(s/s_{\mathrm{g.s.}}) = \Phi(\gamma - 1, s/s_{\mathrm{g.s.}})$ with $\gamma = \delta + 1$.

The best agreement between calculations and the experimental results is obtained using the Stiff2 option ($\gamma = 1$; $\delta = 0$ case). Such calculations are reported in Fig. 2 as shaded area histograms. The dynamical evolution of the system has been determined up to 600 fm/c. Secondary decays of the excited primary fragments produced at the final stage of the CoMD-II calculations are simulated with the GEMINI statistical code [23]. The ensemble of the

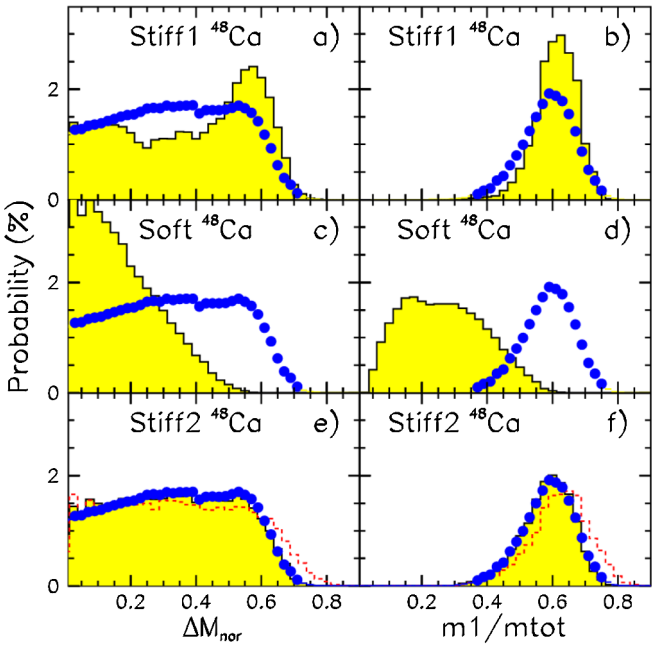

FIG. 3 (color online). CoMD-II + GEMINI calculations (shaded area histogram) and experimental results (dotted histograms) for the ^{48}Ca case for (a),(b) Stiff1 parametrization; (c),(d) Soft parametrization; (e),(f) Stiff2 parametrization, dashed line CoMD-II calculations, without the GEMINI stage.

simulated events has been finally filtered through the angular coverage and detector efficiency of the CHIMERA array. Moreover, the same event selection criteria as in the experimental data have been used. Regardless of some discrepancies at small ΔM_{nor} values, the trend of the data is satisfactorily reproduced. In order to show the sensitivity of our simulated observables to different choices about the stiffness of the density dependence of the symmetry energy, we plot in Fig. 3 the results obtained with ^{48}Ca targets using the Stiff1, Stiff2 and Soft options.

The disagreement with the data for the Stiff1 and Soft options is rather clear. In the Stiff1 and Stiff2 cases, the many-body correlations of CoMD-II generate an attractive interaction as the nuclear density grows, inducing a higher yield of HR. The Soft isovectorial potential maintains and enhances instead the repulsive contribution producing a fragmentation of the source. In the bottom panels in the same figure, the dashed line histograms correspond to the results obtained from CoMD-II simulations performed without the final GEMINI secondary decays of primary excited fragments. The comparison with the shaded area histograms shows that secondary decays shift the peaks in the mass distributions to slightly lower values. However, the overall shape of these distributions remains unaltered.

The mentioned many-body correlations [22] affect significantly the effective strength of the isovectorial interaction. This explains the large changes observed in the mass distributions for the three different parametrizations in Fig. 3. According to the sensitivity shown by the model calculations to the different options used for the form factors describing the symmetry interaction, we can estimate that the $\gamma = 1$ value extracted from the comparison with the experimental data is affected by an error of the order of $\pm 15\%$.

As it has been discussed above, the extracted value of the γ parameter can be affected by many-body correlations characterizing the CoMD-II model. On the other hand, these correlations are responsible for fragment and cluster formation processes. The role played by these many-body correlations in dynamics driven by isospin dependent forces may be better highlighted by comparing our simulations to results obtained with mean-field model approaches using the same strength and form factors.

In summary, we have observed, for the first time, an isotopic effect on the competition between reaction mechanisms producing one or more massive fragments in their final channels at an incident energy of 25 MeV/nucleon. We observe that the production of heavy remnants, essentially deriving from an incomplete fusion mechanism, is enhanced in the case of neutron rich reaction systems, while binary reactions mechanisms dominate in the case of isospin symmetric $N \sim Z$ systems. According to CoMD-II model calculations, the observed isotopic effect is attributed to the interplay between Coulomb and isovectorial interactions. A comparison of the measured mass correlations to CoMD-II model predictions provides a constraint on the stiffness of the nuclear symmetry potential that is found to be characterized by a form factor $F \approx (s/s_{\mathrm{g.s.}})^{\gamma}$ with $\gamma \approx 1.0 \pm 0.15$.

Thanks are due to the INFN Sezione di Catania and INFN LNS staff, respectively, for the invaluable contribution during the setting up of the detector and for the high quality of the delivered beams. Thanks are also due to M. D'Agostino for useful discussions.

*Corresponding author.

[1] Bao-An Li, Lie-Wen Chen, and Che Ming Ko, Phys. Rep. **464**, 113 (2008).
[2] M. Prakash, T. L. Ainsworth, and J. M. Lattimer, Phys. Rev. Lett. **61**, 2518 (1988).
[3] V. Baran, M. Colonna, V. Greco, and M. Di Toro, Phys. Rep. **410**, 335 (2005).
[4] A. W. Steiner, M. Prakash, J. M. Lattimer, and P. J. Ellis, Phys. Rep. **411**, 325 (2005).
[5] I. Bombaci, T. T. S. Kuo, and U. Lombardo, Phys. Rep. **242**, 165 (1994).
[6] M. Prakash *et al.*, Phys. Rep. **280**, 1 (1997).
[7] M. Colonna and M. B. Tsang, Eur. Phys. J. A **30**, 165 (2006).
[8] J. B. Natowitz *et al.*, Phys. Rev. C **52**, R2322 (1995).
[9] S. Levit and P. Bonche, Nucl. Phys. **A437**, 426 (1985).
[10] J. Besprosvany and S. Levit, Phys. Lett. B **217**, 1 (1989).
[11] Zhuxia Li and Min Liu, Phys. Rev. C **69**, 034615 (2004).

[12] Y. J. Zhang, R. K. Su, H. Song, and F. M. Lin, Phys. Rev. C **54**, 1137 (1996).
[13] W. Trautmann *et al.*, Nucl. Phys. **A787**, 575 (2007).
[14] D. Santonocito and Y. Blumenfeld, Eur. Phys. J. A **30**, 183 (2006), and references therein.
[15] F. Amorini *et al.*, Phys. Rev. C **69**, 014608 (2004); M. Papa *et al.*, Phys. Rev. C **68**, 034606 (2003).
[16] H. Morgenstern, W. Bohne, W. Galster, K. Grabisch, and A. Kyanowski, Phys. Rev. Lett. **52**, 1104 (1984); D. A. Bromley, *Treatise on Heavy Ion Science* (Plenum, New York, 1984), Vols. 2,3.
[17] A. Pagano *et al.*, Nucl. Phys. **A734**, 504 (2004).
[18] N. Le Neindre *et al.*, Nucl. Instrum. Methods Phys. Res., Sect. A **490**, 251 (2002); M. Alderighi *et al.*, Nucl. Instrum. Methods Phys. Res., Sect. A **489**, 257 (2002).
[19] S. Aiello *et al.*, Nucl. Instrum. Methods Phys. Res., Sect. A **385**, 306 (1997); S. Aiello *et al.*, Nucl. Instrum. Methods Phys. Res., Sect. A **427**, 510 (1999).
[20] M. Alderighi *et al.*, IEEE Trans. Nucl. Sci. **52**, 1624 (2005).
[21] M. Papa, T. Maruyama, and A. Bonasera, Phys. Rev. C **64**, 024612 (2001); G. Giuliani and M. Papa, Phys. Rev. C **73**, 031601(R) (2006).
[22] M. Papa *et al.*, Phys. Rev. C **75**, 054616 (2007); M. Papa and G. Giuliani, Int. J. Mod. Phys. E **17**, 2320 (2008); M. Papa and G. Giuliani, Eur. Phys. J. A **39**, 117 (2009).
[23] R. J. Charity *et al.*, Nucl. Phys. **A483**, 371 (1988).